Phys. Status Solidi A **207**, No. 7, 1529–1537 (2010) / **DOI** 10.1002/pssa.200983774

physica status solidi a
www.pss-a.com
applications and materials science

Properties of TiO_2-based transparent conducting oxides

Feature Article

Taro Hitosugi*[,1,2], Naoomi Yamada[1], Shoichiro Nakao[1], Yasushi Hirose[1,3], and Tetsuya Hasegawa[1,3]

[1] Kanagawa Academy of Science and Technology (KAST), 213-0012 Kawasaki, Japan
[2] Advanced Institute for Materials Research (WPI-AIMR), Tohoku University, 980-8577 Sendai, Japan
[3] Department of Chemistry, University of Tokyo, 113-0033 Tokyo, Japan

Received 20 July 2009, revised 8 April 2010, accepted 15 April 2010
Published online 9 June 2010

Keywords electrical properties, optical properties, PLD, sputter, structure, TiO_2, transparent conducting oxide

* Corresponding author: e-mail hitosugi@wpi-aimr.tohoku.ac.jp, Phone: +81 22 217 5944, Fax: +81 22 217 5944

The development and properties of titanium dioxide (TiO_2)-based transparent conducting oxides (TCO), which exhibit properties comparable to those of $In_{2-x}Sn_xO_3$ (ITO), are reviewed in this article. An epitaxial thin film of anatase $Ti_{0.94}Nb_{0.06}O_2$ exhibited a resistivity (ρ) of $2.3 \times 10^{-4}\,\Omega\,cm$ and internal transmittance of ~95% in the visible light region. Furthermore, we prepared polycrystalline films with ρ of $6.4 \times 10^{-4}\,\Omega\,cm$ at room temperature on glass substrates by using sputtering. We focus on characteristics unique to TiO_2-based TCO, such as a high refractive index, high transmittance in infrared, and high stability in reducing atmospheres. Possible applications of TiO_2-based TCOs, as well as the mechanism of the transparent conducting properties found in this d-electron-based TCO, are discussed in this review.

Photograph showing TiO_2-based TCO on a transparent plastic film. Note that the film appears greenish due to interference in the film originating from its high refractive index. This high refractive index is one of the unique characteristics of TiO_2-based TCO.

1 Introduction The development of transparent conducting oxides (TCOs) [1] has led to the evolution of a variety of optoelectronic devices, such as flat panel displays (FPDs), touch panels, Si-based solar cells, and light emitting diodes (LEDs) (Fig. 1) [2–4]. In many newly emerging devices, including organic light-emitting diodes (OLEDs), copper indium gallium diselenide (CIGS) solar cells, dye-sensitized solar cells, and blue GaN-based LEDs, TCOs have represented a key component. Currently, $In_{2-x}Sn_xO_3$ (ITO) and F-doped SnO_2 are the most widely used TCOs because of their excellent transparent conducting properties [5–7] and ease of fabrication.

There remains, however, a strong demand for the development of new TCOs, for two major reasons. One is the industrial need for high-efficiency optoelectronic devices. The tuning of TCO properties can greatly improve device performance. For example, the use of a TCO with a refractive index matching with that of GaN would significantly increase the external quantum efficiency of blue GaN LEDs [8–10]. Furthermore, careful selection of a TCO, considering its transmittance in the infrared region and work function, would improve the efficiency of solar cells [11] and OLEDs.

The second major motivation for the development of new TCOs involves scarcity. Indium (In), which is categorized as a

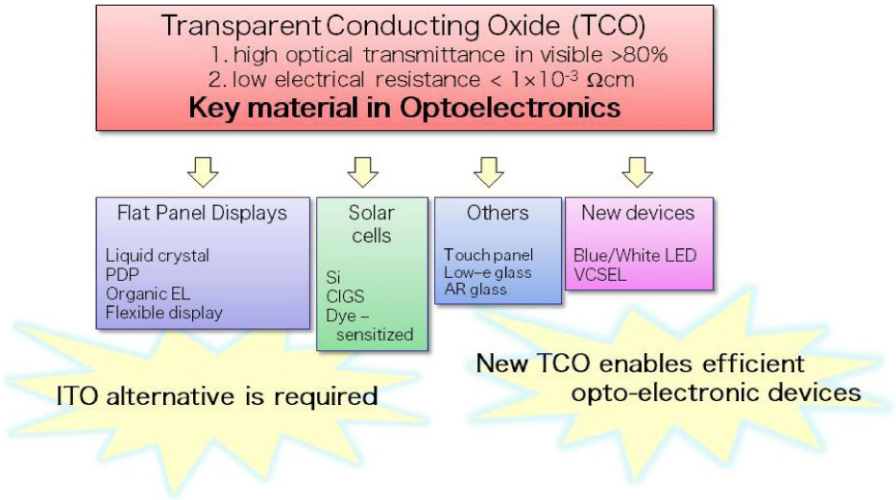

Figure 1 (online color at: www.pss-a.com) Widespread usage of TCO.

rare metal, faces an unstable supply because of its rapidly expanding consumption due to commercialization of wide-area FPDs. This has stimulated the search for new TCO materials based on more abundant elements, as well as efforts toward the reduction of In use and In recycling. Although ZnO is a promising alternative to ITO [12], it remains necessary to explore new TCO materials in order to enable the wider application of TCOs.

In this article, we review the development and properties of a new TCO, anatase $Ti_{1-x}Nb_xO_2$ (TNO) [13, 14], which exhibits electrical and optical properties comparable to those of ITO. Anatase titanium dioxide (TiO_2) is a promising mother compound of TCO, characterized by a wide band gap (3.2 eV) [15] and an effective mass of approximately 1 m_0 (m_0: free electron mass) [16]. Furthermore, TNO has properties that ITO does not possess, such as a high refractive index, high transmittance in the infrared region, and high chemical stability especially in a reducing atmosphere. These properties may allow the use of TNO in new, high-efficiency optoelectronic devices. Moreover, Ti, a major constituent of TNO, is much more abundant in the earth's crust than In, by a factor of roughly 10^5 [17].

This article is organized as follows. In the next section, we briefly introduce the basic electronic properties and film growth of TiO_2. The transparent conducting properties of TNO are described in Section 3. Section 4 presents an application-oriented topic: the deposition of polycrystalline TiO_2-based transparent conductors on glass substrates. In Section 5, we discuss the differences between TNO and conventional TCOs in terms of the mechanism that gives rise to transparent conductivity. Finally, in Section 6, we discuss the future prospects of TNO.

2 Titanium dioxide (TiO_2) TiO_2 has been extensively studied because of its usefulness in a wide variety of applications, including catalysis [18], pigments, and sensors [19]. Recently, TiO_2 has attracted considerable attention as a material for use in electronic devices, such as high-k materials [20], resistive random access memory (RRAM) [21], and diluted magnetic semiconductors for room-temperature spintronic devices [22]. Reviews of the properties of TiO_2 in relation to its applications can be found elsewhere [23, 24].

Among the many polytypes of TiO_2, the most technologically important crystal structures are rutile and anatase (Fig. 2). Both rutile and anatase, with tetragonal symmetry, can be described as a network of TiO_6 octahedra, but the two structures differ in the distortion and linkage of these octahedra. In the anatase structure, each octahedron is in contact with eight neighbors (four shared edges and four shared corners), as shown in Fig. 2c, while the coordination number of rutile is 10 (two shared edges and eight shared corners) (Fig. 2d).

Anatase TiO_2 tends to incorporate oxygen vacancies, which can be expressed as $TiO_{2-\delta}$. The amount of oxygen vacancies δ can be controlled by adjusting film growth and/or annealing conditions. The oxygen vacancies generate n-type carriers in the Ti-3d conduction band, so that the resistivity (ρ) of TiO_2 can be decreased by introducing oxygen vacancies. However, oxygen-deficient $TiO_{2-\delta}$ films lose their transparency, and thus cannot be used as a TCO. In addition to the introduction of oxygen vacancies, the substitution of Nb for Ti could introduce charge carriers. Indeed, it is known that Nb-doping to rutile TiO_2 decreases ρ by a factor of more than 5500 [25], although the minimum ρ value ($\sim 10^{-2}\,\Omega$ cm at room temperature) [26, 27] is insufficient for TCO applications due to the low electron mass ($\ll 1\,m_0$) in rutile [28].

Anatase, which has a higher mobility than rutile, is more suited to TCO applications. The transport properties of anatase, however, have not been thoroughly studied, since anatase is a thermodynamically metastable structure, and it is difficult to grow single crystals in bulk form. Lévy and coworkers [29] first reported single-crystal growth of anatase using chemical vapor transport. They measured the optical and transport properties, and obtained ρ of the order of

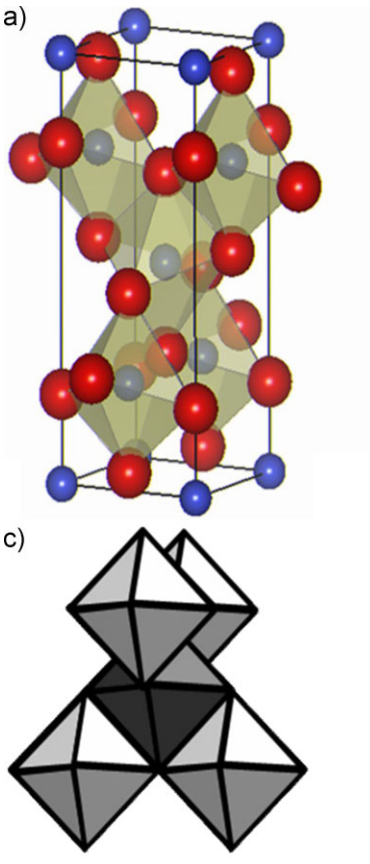

Figure 2 (online color at: www.pss-a.com) Crystal structures of (a) anatase and (b) rutile. Red and blue spheres denote O and Ti atoms, respectively, and schematics of the TiO_6-octahedra networks in (c) anatase and (b) rutile.

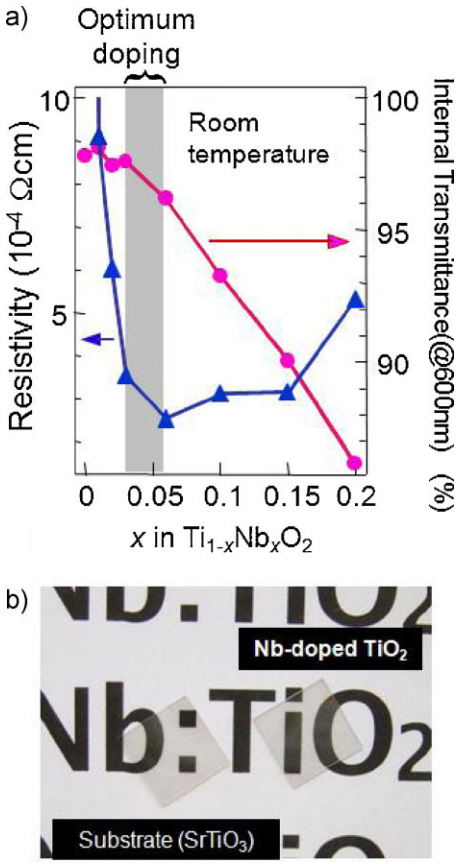

Figure 3 (online color at: www.pss-a.com) (a) Resistivity and internal transmittance (at a wavelength of 600 nm) of $Ti_{1-x}Nb_xO_2$. Both a high electrical conductivity and a high optical transmittance were obtained for $0.03 \leq x \leq 0.06$. (b) A photograph of a $SrTiO_3$ substrate and a $Ti_{0.94}Nb_{0.06}O_2$ epitaxial thin film on that substrate.

$10^{-1}\,\Omega\,cm$ with an electron mobility exceeding $600\,cm^2/Vs$ at 50 K [30]. Single crystals of Nb-doped anatase TiO_2 were investigated by Mulmi et al. [31], who reported ρ values of $\sim 5 \times 10^{-2}\,\Omega\,cm$. Their ρ versus temperature (ρ–T) curve exhibited semiconducting behavior, possibly due to the low Nb concentration.

Anatase TiO_2 films have been fabricated by various techniques [32, 33]. These include sputtering, pulsed laser deposition (PLD), molecular beam epitaxy, chemical vapor deposition, sol–gel, and spray pyrolysis. However, to our knowledge, highly conducting TNO films have been synthesized only by sputtering or PLD, so far.

3 Transparent conducting properties A dramatic nonmetal–metal transition takes place when doping anatase TiO_2 with Nb. Figure 3a plots the ρ values of $Ti_{1-x}Nb_xO_2$ epitaxial thin films grown by PLD on $SrTiO_3$(100) or $LaAlO_3$(100) substrates [13, 14]. X-ray diffraction (XRD) measurements confirmed that the films were single-phase crystals, free of any impurity phases. Undoped anatase TiO_2 exhibited ρ of the order of $10^{-1}\,\Omega\,cm$, while Nb doping caused a marked decrease in ρ, with a minimum ρ value of $2 \times 10^{-4}\,\Omega\,cm$ at 300 K ($x = 0.06$). The optimal ρ values were as low as $2\text{–}3 \times 10^{-4}\,\Omega\,cm$, and were comparable to those of conventional ITO films [5].

The internal transmittance at 600 nm, as evaluated from optical absorption/reflection measurements, gradually decreased with increasing Nb doping, mainly due to light absorption by the charge carriers. As seen from Fig. 3a, both high electrical conductivity and high optical transmittance can be achieved in the range of $0.03 \leq x \leq 0.06$. Figure 3b shows photographs of a $SrTiO_3$ substrate and Nb-doped TiO_2 (TNO) film grown on a $SrTiO_3$ substrate, demonstrating the high optical transparency of TNO.

These highly conductive TNO films are typical degenerate semiconductors: the doped Nb atoms exist as Nb^{5+} ions, and release conduction electrons with high efficiency. There was a fairly linear relationship between n_e and x, up to an x value of ~ 0.06 (Fig. 4a). n_e was nearly equal to n_{Nb}, where n_{Nb} is the density of Nb. This implies that Nb ions release conduction electrons with an efficiency of $\sim 90\%$, up to $x = 0.06$. At higher doping levels ($x > 0.06$), the ionization efficiency was slightly suppressed. The Hall mobility, μ_H, increased as the temperature (T) was lowered (Fig. 4b),

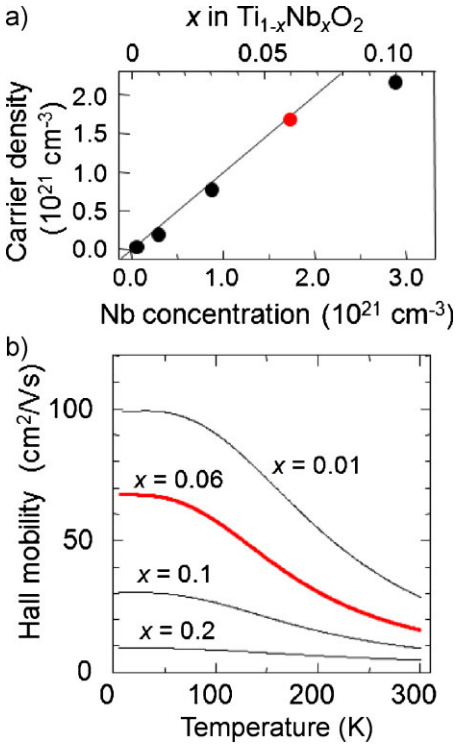

Figure 4 (online color at: www.pss-a.com) (a) Carrier density at 300 K as a function of Nb concentration and x. The carrier density should lie on the solid line when the Nb activation efficiency is 100%. Note that the carrier density was almost equal to the Nb concentration up to $x = 0.06$, indicating a high Nb activation efficiency. (b) Hall mobility as a function of temperature. The Hall mobility increased with decreasing temperature, indicating a metallic temperature dependence.

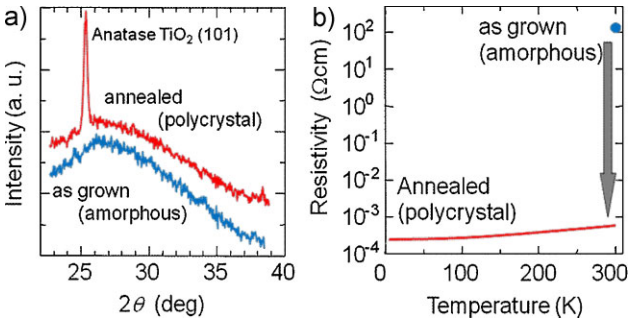

Figure 5 (online color at: www.pss-a.com) (a) X-ray diffraction patterns of a $Ti_{0.94}Nb_{0.06}O_2$ film before (as-grown, amorphous) and after H_2 annealing at 500 °C. The amorphous film crystallized upon annealing. (b) Resistivity of as-grown amorphous and annealed films. The annealed film had a positive temperature coefficient, indicative of metallic behavior.

which is similar to the behavior of a typical metal. Therefore, at room temperature, the resistivity of TNO is dominated by phonon scattering. The films within the optimal x region ($0.03 \leq x \leq 0.06$) had μ_H (300 K) values around 20 cm^2/Vs, which were approximately half that of ITO with the same ρ [34] In terms of electron mobility, recent studies report films exceeding 100 cm^2/Vs for In oxide by doping Mo [35], Zr [36], or H [37].

After the first report on the PLD growth of $Ti_{0.94}Nb_{0.06}O_2$ films by Furubayashi et al., several groups have studied the deposition of TNO epitaxial thin films using PLD [38, 39] or sputtering [40, 41] to obtain highly transparent conducting properties. Anatase films doped with Ta had similar transparent conducting properties [42]. In contrast, W-doped anatase, in which each dopant ion (W^{6+}) was expected to release two electrons, was found to be less conductive than Nb- or Ta-doped anatase [43].

4 Polycrystalline films on glass substrates

Considerable efforts have been devoted to the deposition of TCO films on glass, because of the increasing technological demands for FPDs and solar cells. We have succeeded in preparing TNO films on glass using PLD to obtain $\rho = 4.6 \times 10^{-4}\,\Omega\,cm$ [44], which meets the practical usage requirement for TCOs: $\rho < 10^{-3}\,\Omega\,cm$.

These polycrystalline films were prepared on glass through crystallization of an amorphous phase (Fig. 5a). The crystallization process was accompanied by a 10^6-fold drop in ρ (Fig. 5b). We applied this technique to TNO films sputter-deposited on glass substrates, and obtained a ρ of $6.4 \times 10^{-4}\,\Omega\,cm$ at room temperature [45]. Using a similar process, Sato et al. [46] recently obtained transparent conducting TNO films using a DC sputtering method.

The procedure for fabricating TNO films by sputtering was as follows. (1) Amorphous $Ti_{0.94}Nb_{0.06}O_2$ films were deposited using a commercial sputtering apparatus (Canon-ANELVA, E-200S) on unheated nonalkali glass (Corning 1737) substrates (Fig. 6a). A sintered pellet with a nominal composition of $Ti_{0.94}Nb_{0.06}O_{2-\delta}$ was used as a sputtering target, and the deposition time was adjusted to obtain films with thicknesses of ~200 nm. (2) The as-grown films were then annealed in vacuum using a rapid thermal annealing furnace, in which the annealing temperature was raised to 500 °C within 5 min (Fig. 6b). Annealing for 5 min was sufficient to obtain highly conducting films. The annealing furnace was evacuated to 10^{-4} Torr to remove residual oxygen from the furnace. Several obtained films are shown in Fig. 6c and d. Note that the films are colored due to optical interference.

The most important process parameter to obtain high-conductivity TNO films is the control of oxygen stoichiometry in the films during sputtering. Starting with an oxygen-deficient $Ti_{0.94}Nb_{0.06}O_{2-\delta}$ target, with a shiny black color, is essential. The $Ti_{0.94}Nb_{0.06}O_2$ target was reduced by annealing to introduce oxygen vacancies. It is also possible to use Nb-doped TiO or Ti_2O_3 as a sputtering target [47]. The oxygen partial pressure during deposition should be maintained around 1×10^{-3} Pa to control the oxygen content of the films precisely. The annealing conditions also influence the electrical properties of the TNO. Annealing in air at 600 °C yields insulating films.

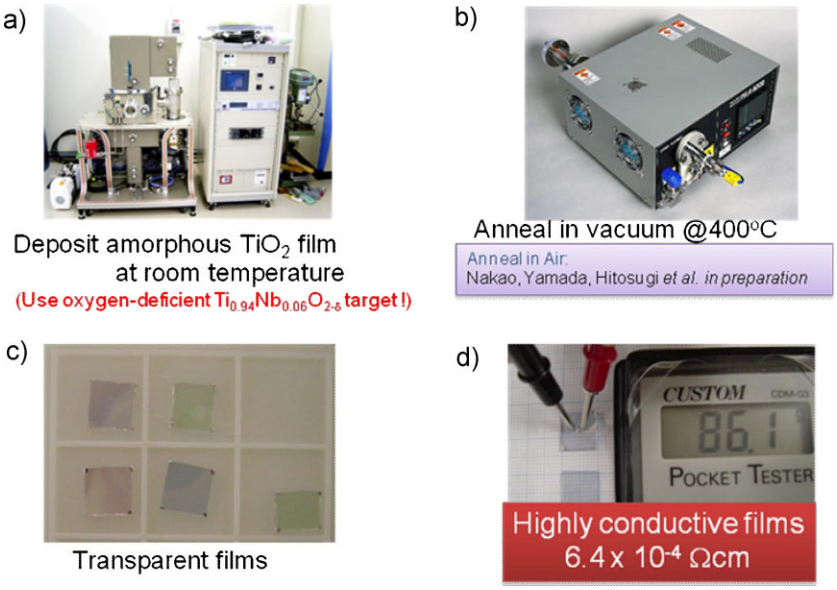

Figure 6 (online color at: www.pss-a.com) Preparation of TiO_2-based TCO on a glass substrate. (a) Deposition of an amorphous TiO_2 film at room temperature by sputtering. (b) Annealing of the amorphous film in vacuum at 300–600 °C. Annealing for 5 min is sufficient to obtain highly conductive films. Recently, conducting films were obtained after annealing in air, with $x < 0.03$ films. (c) Photographs of films on glass. The films appear colored due to an interference effect. (d) Demonstration of the excellent conductivity of TiO_2-based TCO films.

The minimum ρ value achieved by this annealing process was $8 \times 10^{-4}\,\Omega\,\mathrm{cm}$, which is very low for a polycrystalline transition metal oxide [48]. By introducing a seed layer, which is a TNO but deposited at different oxygen partial pressure during deposition, we obtained films with a ρ of $6.4 \times 10^{-4}\,\Omega\,\mathrm{cm}$ [45]. The seed layer acted as a template for anatase growth, and also served as a crystal growth center, resulting in suppression of crystallization temperature. We successfully obtained conductive TNO films ($\rho \sim 1.6 \times 10^{-3}\,\Omega\,\mathrm{cm}$) on transparent polyimide films at an annealing temperature of 250°C. Table 1 summarizes the growth conditions and obtained ρ values [49, 50]. Very recently, we succeeded in preparing conductive films by annealing amorphous films in air at 300–400°C (S. Nakao et al., unpublished data.).

Surprisingly, polycrystalline TNO films with ρ on the order of $10^{-4}\,\Omega\,\mathrm{cm}$ also exhibit metallic ρ–T behavior. This suggests that the carrier transport is relatively unaffected by grain boundaries. Furthermore, the n_e value was as high as $\sim 1.6 \times 10^{21}\,\mathrm{cm}^{-3}$, from which the ionization efficiency was estimated to be ~90%. These results indicate that the Nb dopants were substituted for Ti sites in anatase without segregation, even in polycrystalline films. TNO films in both epitaxial and polycrystalline form had a high activation efficiency compared with other conventional TCOs (typically < 50% in the case of ITO) [51–53]. As for electron mobility, Hirose et al. [54] revealed that the anisotropy of mobility in anatase TiO_2 would reduce the overall electron mobility of a polycrystalline TNO film, since electrons must conduct along the low-mobility c-axis direction in polycrystalline films.

Transmittance (T_r) and reflectance (R) spectra of a polycrystalline TNO film after annealing (thickness ≈200 nm) demonstrates the high transparency of TNO (Fig. 7a). The T_r value was 60–80% throughout the wavelength range of 400–1500 nm, somewhat lower than that of a typical ITO film. This is due to the relatively high refractive index of anatase TNO (~2.4 at 500 nm), which tends to enhance R and suppress T_r. The absorptance (A) in the visible region, calculated from the equation $A = 1 - (T_r + R)$, was below 5% (Fig. 7b).

In addition to film preparation from the amorphous state, the direct deposition of polycrystalline films by sputtering is also possible. At present, the directly grown films have a ρ of $1 \times 10^{-3}\,\Omega\,\mathrm{cm}$, which is higher than that of TNO films prepared from amorphous films [55].

5 Mechanism of transparent conductivity We performed first-principles band structure calculations with the generalized gradient approximation (GGA) [56], and

Table 1 Growth and annealing conditions and resistivity values obtained for polycrystalline Nb-doped anatase TiO_2 thin films. $f(O_2)$ is a measure of oxygen partial pressured during deposition (see Ref. [45]).

composition, $Ti_{1-x}\,Nb_xO_2$		substrate	$f(O_2)$		annealing condition		resistivity
target	film		top layer	seed fayer	temperature	atmosphere	
$x = 0.06$	–	nonalkaline glass	0.05%	5%	400 °C	vacuum	$6.4 \times 10^{-4}\,\Omega\,\mathrm{cm}$
$x = 0.06$	–	nonalkaline glass	0.05%	no seed layer	400 °C	vacuum	$7.6 \times 10^{-4}\,\Omega\,\mathrm{cm}$
$x = 0.037$	–	polyimide	0.05%	5%	300 °C	H_2	$1.9 \times 10^{-3}\,\Omega\,\mathrm{cm}$

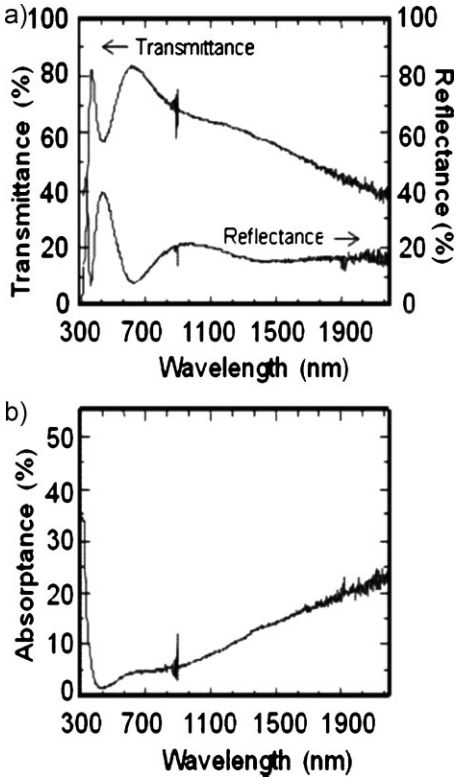

Figure 7 (a) Transmittance, reflectance, and (b) absorptance spectra of a typical anatase $Ti_{0.94}Nb_{0.06}O_2$ film on a glass substrate.

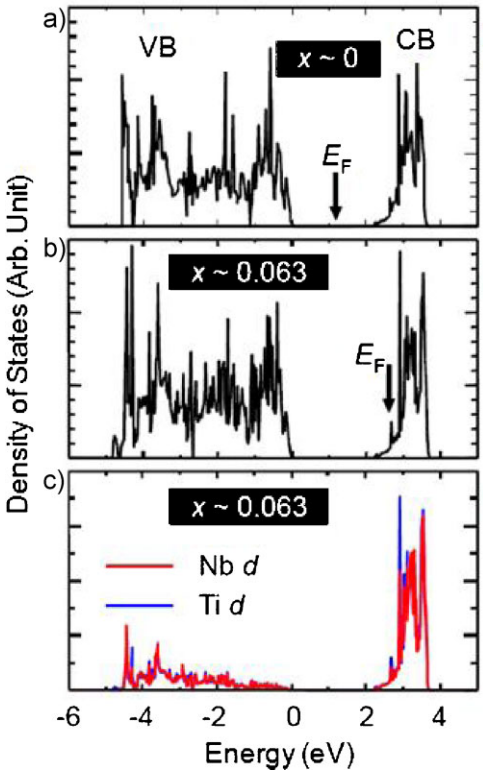

Figure 8 (online color at: www.pss-a.com) Density of states calculated for (a) undoped and (b) Nb-doped anatase; (c) partial DOS. The origin of energy ($E = 0$) corresponds to the top of the valence band (VB). Note that the Fermi energy (E_F) shifts to higher energy side upon Nb doping.

compared these with resonant photoemission measurements [57].

The density of states (DOS) as a function of electron energy calculated for undoped anatase TiO_2 exhibited a band gap of about 2.24 eV (Fig. 8a), which was somewhat narrower than the empirical value of 3.2 eV. This underestimation of the band gap is a well-known limitation of GGA calculations. The Fermi energy (E_F) was in the middle of the band gap, reflecting the insulating behavior of pure anatase TiO_2.

In contrast, a total DOS profile calculated for $Ti_{1-x}Nb_xO_2$ indicated that the Fermi energy (E_F) was located inside the conduction band (Fig. 8b), implying that $Ti_{1-x}Nb_xO_2$ can be described as a normal metal. In this calculation, the central Ti atom in a super cell was substituted by Nb, corresponding to a doping content x of $\sim$0.0625. The result was consistent with the experimentally observed positive $d\rho/dT$ and the temperature-independent n_e [13]. Furthermore, no impurity state was observed in the in-gap region, which explains the high optical transparency of TNO in the visible region.

Partial DOS profiles of Ti 3d and Nb 4d states above E_F had essentially identical shapes (Fig. 8c), indicating that the Nb 4d orbital spread over the entire region of the conduction band. This suggests that Nb was strongly hybridized with Ti. As a consequence of the strong Ti–Nb hybridization, each Nb atom released one electron to the conduction band, resulting in the high n_e ($>10^{21}$ cm^{-3}). This was in contrast to Nb-doped rutile TiO_2 which showed semiconducting carrier transport with $d\rho/dT < 0$ as a result of the formation of shallow Nb impurity states [58].

Ti 2p–3d resonant photoemission spectroscopy clearly revealed a finite DOS at E_F, indicating that the states were contributed to by Ti orbitals. Figure 9 shows off-resonant ($h\nu = 600$ eV) and Ti 2p–3d resonant ($h\nu = 461.2$ eV) spectra of $Ti_{0.94}Nb_{0.06}O_2$ near the band gap. The on-resonant spectrum exhibited a clear peak at E_F, corresponding to the bottom of the Ti 3d conduction band, whereas the spectral weight observed in the off-resonant spectra near E_F was negligible. This demonstrates that the conduction electrons had a d-electron nature, as predicted by the band calculations. Furthermore, we could not detect any impurity states within the band gap, which was consistent with the GGA calculations.

The above discussions focused on carrier generation in TNO. From the viewpoint of transparency, however, a large n_e due to a high ionization efficiency is unfavorable, because carriers absorb light, decreasing the optical transmittance. The trade-off between electrical conductivity and transparency is a crucial issue for TCOs [59].

Next, we discuss the transparency of TNO in the visible region (wavelengths of 400–800 nm). At wavelengths shorter than 400 nm, a strong inter-band absorption across

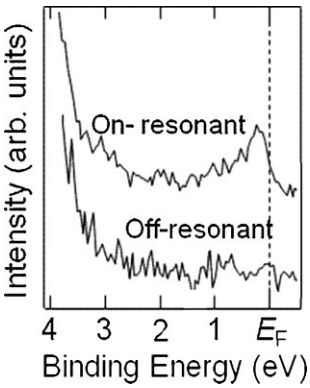

Figure 9 Off-resonant ($h\nu = 600$ eV) and Ti 2p–3d resonant ($h\nu = 461.2$ eV) X-ray photoemission spectra of anatase $Ti_{0.94}Nb_{0.06}O_2$.

the fundamental band gap occurs. At longer wavelengths in the infrared region, free carriers absorb light, and the transmission characteristics are determined by the plasma wavelength, λ_p [60]:

$$\lambda_p = 2\pi c\left(\frac{\varepsilon_0\varepsilon_\infty m^*}{n_e e^2}\right)^{\frac{1}{2}} \quad (1)$$

where ε_0, ε_∞, c, m^*, and e denote the dielectric constant of vacuum, the high-frequency permittivity, the speed of light, the effective mass, and the electronic charge, respectively. The maximum absorption occurred at λ_p, and light with wavelengths shorter than λ_p could pass through the film. Thus, λ_p should be much larger than 800 nm to ensure sufficient transparency in the visible region (Fig. 10a).

The value of λ_p decreases as the value n_e is increased, causing the absorption of visible light to become significant. In conventional TCOs, n_e is adjusted to less than 1×10^{21} cm^{-3}, and this relatively low n_e is compensated by a high electron mobility to increase electron conductivity (Fig. 10b). In contrast, n_e could easily exceed 10^{21} cm^{-3} in a TNO film, while maintaining excellent transparency. This can be explained by the relatively large ε_∞ of TiO_2. That is, as can be seen from Eq. (1), a larger ε_∞ results in a red-shift of λ_p, which restores transparency in the visible light region. The reported ε_∞ of 5.9 [61] for TiO_2 is almost 1.5 times that of ITO, which typically has an ε_∞ of ~4 [62, 63].

In addition to the high ε_∞, a large m^* also plays an important role in the transparency of TNO. Hirose et al. [64] discussed effective mass anisotropy in $Ti_{0.94}Nb_{0.06}O_2$ epitaxial thin films on the basis of Drude analysis, and reported m^* values along the a- and c-axis as $m_a^* \sim 0.6\,m_0$ and $m_c^* \sim 3.3\,m_0$, respectively. In contrast, ITO is known to have a smaller m^*, ~$0.3\,m_0$ [65]. Note that the transmittance of TNO in the infrared region is higher than that of ITO with the same n_e. This is of great advantage in certain applications, such as solar cells [66].

A large dielectric constant ε is thought to strongly affect the transport properties of TNO. Electronic charges associated with impurities are effectively screened by carriers (Thomas–Fermi screening), and the screening length is proportional to $\varepsilon^{1/2}$. Thus, a larger dielectric constant contributes to the suppression of carrier scattering by impurities. This explains why TNO maintains a high mobility, even when it is heavily doped with Nb.

6 Prospects for applications For TiO_2-based TCOs, it is of crucial importance to find applications which exploit their unique characteristics. As mentioned earlier, TNO has remarkable properties that ITO cannot achieve, such as a high refractive index (~2.4 at a wavelength of 500 nm), high transmittance in the infrared region, and high stability in a reducing atmosphere. Development of optoelectronic devices utilizing such properties would expand the use of TCOs and potentially create new markets. For example, electrodes for blue LEDs and solar cells are promising applications of TNO. In terms of the chemical stability, film stability under a hydrogen plasma may be an advantage over ITO, [67] since TiO_2 is reported to be resistant to atomic hydrogen

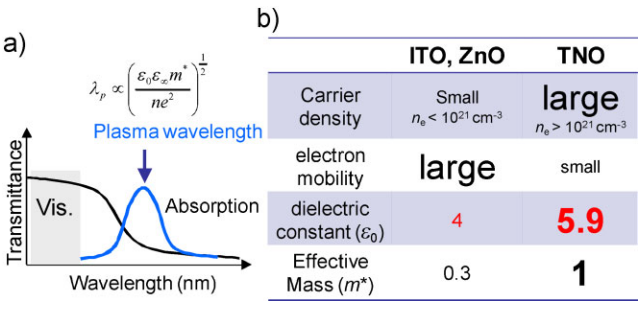

Figure 10 (online color at: www.pss-a.com) (a) Transmittance and absorption spectra of a transparent conductor. The plasma wavelength must be greater than 800 nm to ensure transparency in the visible range. (b) Comparison of material parameters between conventional TCOs (ITO, ZnO, SnO_2, etc.) and the TiO_2-based TCO. See the text for the references to the ε_∞ and m^* values.

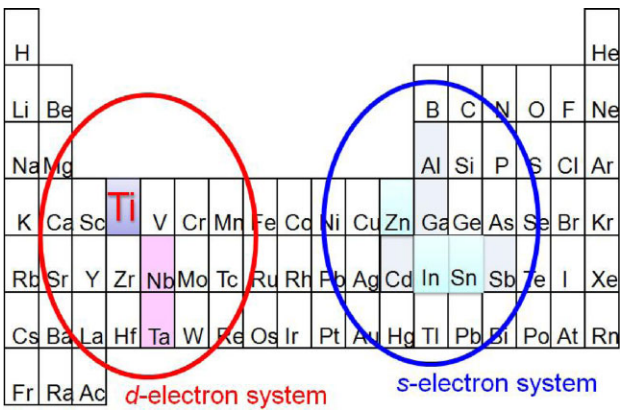

Figure 11 (online color at: www.pss-a.com) Periodic table showing elements used for transparent conductors. Note that Ti is located on the left-hand side of the periodic table, indicating the importance of d electrons.

during depositing amorphous Si for solar cells [68, 69]. Furthermore, TNO is a d-electron based TCO (Fig. 11), in sharp contrast to conventional TCOs based on s or p electrons. Combining TCO properties with spins associated with d-electrons might provide a new concept for spintronic devices.

Further improvement of resistivity and transmittance is required for TNO. A better understanding of carrier transport in polycrystalline TNO films, with the aid of theoretical predictions, would pave the way towards post-ITO materials.

7 Conclusions We have reviewed the development and properties of anatase TiO_2-based TCOs. Epitaxial films of Nb-doped TiO_2 (TNO) exhibited a low resistivity of $\sim 2 \times 10^{-4}\,\Omega\,\mathrm{cm}$ and high optical transmittance in the visible region. We successfully prepared highly conductive TNO polycrystalline films on glass substrates by sputtering. These polycrystalline films were transparent, with an absorption of less than 10%. These results should encourage the practical use of polycrystalline TNO films as wide-area transparent electrodes. Future applications of TNO should utilize its unique characteristics to enable new fields of application. Given that TNO is a d-electron-based TCO, we believe that other d-electron based oxides should be the subject of intensive study in the search for new TCOs.

Acknowledgements We gratefully acknowledge our collaborators, Profs. M. Oshima, H. Kumigashira, K. Yamashita, H. Kamisaka (University of Tokyo), and Prof. Y. Furubayashi (Kanazawa Institute of Technology). This work was supported by MEXT (Ministry of Education, Culture, Sports, Science and Technology), Elements Science and Technology Project, the Global COE Program for Chemistry Innovation, and NEDO (New Energy and Industrial Technology Development Organization).

References

[1] D. S. Ginley and C. Bright, MRS Bull. **25**, 15 (2000).
[2] E. Fortunato, D. Ginley, H. Hosono, and D. C. Paine, MRS Bull. **32**, 242 (2007).
[3] E. Fortunato, L. Raniero, L. Silva, A. Gonçalves, A. Pimentel, P. Barquinha, H. Águas, L. Pereira, G. Gonçalves, I. Ferreira, E. Elangovan, and R. Martins, Sol. Energy Mater. Sol. Cells **92**, 1605 (2008).
[4] H. L. Hartnagel, A. L. Dawar, A. K. Jain, and C. Jagadish, Semiconducting Transparent Thin Films (Institute of Physics, Bristol, UK, 1995).
[5] C. A. Pan and T. P. Ma, Appl. Phys. Lett. **37**, 163 (1980).
[6] I. Hamberg and C. G. Granqvist, J. Appl. Phys. **60**, R123 (1986).
[7] S. Calnan and A. N. Tiwari, Thin Solid Films **518**, 1839 (2010).
[8] S. Pimputkar, J. S. Speck, S. P. DenBaars, and S. Nakamura, Nature Photonics **3**, 180 (2009).
[9] J.-H. Lim, D.-K. Hwang, H.-S. Kim, J.-Y. Oh, J.-H. Yang, R. Navamathavan, and S.-J. Park, Appl. Phys. Lett. **85**, 6191 (2004).
[10] J. Kasai, T. Hitosugi, M. Moriyama, K. Goshonoo, N. L. H. Hoang, S. Nakao, N. Yamada, and T. Hasegawa, J. Appl. Phys. **107**, 053110 (2010).
[11] M. Kambe, K. Sato, D. Kobayashi, Y. Kurokawa, S. Miyajima, M. Fukawa, N. Taneda, A. Yamada, and M. Konagai, Jpn. J. Appl. Phys. **45**, L291 (2006).
[12] T. Minami, Mater. Res. Bull. **25**, 38 (2000).
[13] Y. Furubayashi, T. Hitosugi, Y. Yamamoto, K. Inaba, G. Kinoda, Y. Hirose, T. Shimada, and T. Hasegawa, Appl. Phys. Lett. **86**, 252101 (2005).
[14] T. Hitosugi, Y. Furubayashi, A. Ueda, K. Itabashi, K. Inaba, Y. Hirose, G. Kinoda, Y. Yamamoto, T. Shimada, and T. Hasegawa, Jpn. J. Appl. Phys. **44**, L1063 (2005).
[15] H. Tang, H. Berger, P. E. Schmid, F. Lévy, and G. Burri, Solid State Commun. **23**, 161 (1977).
[16] H. Tang, K. Prasad, R. Sanjines, P. E. Schmid, and F. Lévy, J. Appl. Phys. **75**, 2042 (1994).
[17] S. R. Taylor and S. H. McLennan, The Continental Crust: Its Composition and Evolution (Blackwell, Oxford, 1985), p. 312.
[18] A. Fujishima and K. Honda, Nature **37**, 238 (1972).
[19] O. Carp, C. L. Huisman, and A. Reller, Prog. Solid State Chem. **32**, 33 (2004).
[20] A. I. Kingon, J.-P. Maria, and S. K. Streiffer, Nature **406**, 1032 (2000).
[21] M. Fujimoto, H. Koyama, M. Konagai, Y. Hosoi, K. Ishihara, S. Ohnishi, and N. Awaya, Appl. Phys. Lett. **89**, 223509 (2006).
[22] Y. Matsumoto, M. Murakami, T. Shono, T. Hasegawa, T. Fukumura, M. Kawasaki, P. Ahmet, T. Chikyow, S. Koshihara, and H. Koinuma, Science **291**, 534 (2001).
[23] K. Hashimoto, H. Irie, and A. Fujishima, Jpn. J. Appl. Phys. **44**, 8269 (2005).
[24] T. Fukumura, H. Toyosaki, and Y. Yamada, Semicond. Sci. Technol. **20**, S103 (2005).
[25] F. A. Grant, Rev. Mod. Phys. **31**, 646 (1959).
[26] Y. Furubayashi, T. Hitosugi, and T. Hasegawa, Appl. Phys. Lett. **88**, 226103 (2006).
[27] S. X. Zhang, D. C. Kundaliya, W. Yu, S. Dhar, S. Y. Young, L. G. Salamanca-Riba, S. B. Ogale, R. D. Vispute, and T. Venkatesan, J. Appl. Phys. **102**, 013701 (2007).
[28] D. C. Cronemeyer, Phys. Rev. **87**, 876 (1952).
[29] H. Berger, H. Tang, and F. Lévy, J. Cryst. Growth **130**, 108 (1993).
[30] L. Forro, O. Chauvet, D. Emin, Z. Zuppiroli, H. Berger, and F. Levy, J. Appl. Phys. **75**, 633 (1994).
[31] D. D. Mulmi, T. Sekiya, N. Kamiya, S. Kurita, Y. Murakami, and T. Kodaira, J. Phys. Chem. Solids **65**, 1181 (2004).
[32] D. P. Norton, Mater. Sci. Eng. R **43**, 139 (2004).
[33] S. A. Chambers, Surf. Sci. Rep. **39**, 105 (2000).
[34] Y. Shigesato, D. C. Paine, and T. E. Haynes, J. Appl. Phys. **73**, 3805 (1993).
[35] S. Parthiban, K. Ramamurthi, E. Elangovan, R. Martins, and E. Fortunato, Appl. Phys. Lett. **94**, 212101 (2009).
[36] T. Koida and M. Kondo, Appl. Phys. Lett. **89**, 082104 (2006).
[37] T. Koida, M. Kondo, K. Tsutsumi, A. Sakaguchi, M. Suzuki, and H. Fujiwara, J. Appl. Phys. **107**, 033514 (2010).
[38] D. Kurita, S. Ohta, K. Sugiura, H. Ohta, and K. Koumoto, J. Appl. Phys. **100**, 096105 (2006).
[39] S. X. Zhang, S. Dhar, W. Yu, H. Xu, S. B. Ogale, and T. Venkatesan, Appl. Phys. Lett. **91**, 112113 (2007).
[40] M. A. Gillispie, M. F. A. M. van Hest, M. S. Dabney, J. D. Perkins, and D. S. Ginley, J. Appl. Phys. **101**, 033125 (2007).

[41] M. S. Dabney, M. F. A. M. van Hest, C. W. Teplin, S. P. Arenkiel, J. D. Perkins, and D. S. Ginley, Thin Solid Films **516**, 4133 (2008).
[42] T. Hitosugi, Y. Furubayashi, A. Ueda, K. Itabashi, K. Inaba, Y. Hirose, G. Kinoda, Y. Yamamoto, T. Shimada, and T. Hasegawa, Jpn. J. Appl. Phys. **44**, L1063 (2005).
[43] U. Takeuchi, A. Chikamatsu, T. Hitosugi, H. Kumigashira, M. Oshima, Y. Hirose, T. Shimada, and T. Hasegawa, J. Appl. Phys. **107**, 023705 (2010).
[44] T. Hitosugi, A. Ueda, S. Nakao, Y. Furubayashi, N. Yamada, Y. Hirose, T. Shimada, and T. Hasegawa, Appl. Phys. Lett. **90**, 212106 (2007).
[45] N. L. H. Hoang, N. Yamada, T. Hitosugi, J. Kasai, S. Nakao, T. Shimada, and T. Hasegawa, Appl. Phys. Express **1**, 115001 (2008).
[46] Y. Sato, H. Akizuki, T. Kamiyama, and Y. Shigesato, Thin Solid Films **516**, 5758 (2008).
[47] N. Yamada, T. Hitosugi, J. Kasai, N. L. H. Hoang, S. Nakao, Y. Hirose, T. Shimada, and T. Hasegawa, Thin Solid Films **518**, 3101 (2010).
[48] N. Tsuda, K. Nasu, A. Fujimori, and K. Shiratori, Electronic Conduction in Oxides (Springer, Berlin, 2000).
[49] T. Hitosugi, N. Yamada, N. L. H. Hoang, J. Kasai, S. Nakao, T. Shimada, and T. Hasegawa, Thin Solid Films **517**, 3106 (2009).
[50] N. Yamada, T. Hitosugi, N. L. H. Hoang, Y. Furubayashi, Y. Hirose, T. Shimada, and T. Hasegawa, Jpn. J. Appl. Phys. **46**, 5275 (2007).
[51] N. Yamada, I. Yasui, Y. Shigesato, H. Li, Y. Ujihira, and K. Nomura, Jpn. J. Appl. Phys. **39**, 4158 (2000).
[52] H. Köstlin, R. Jost, and W. Lems, Phys. Status Solidi A **29**, 87 (1975).
[53] J.-C. Manifacier, L. Szepessy, J. F. Bresse, M. Perotin, and R. Stuck, Mater. Res. Bull. **14**, 163 (1079).
[54] Y. Hirose, N. Yamada, S. Nakao, T. Hitosugi, T. Shimada, and T. Hasegawa, Phys. Rev. B **79**, 165108 (2009).
[55] N. Yamada, T. Hitosugi, J. Kasai, N. L. H. Hoang, S. Nakao, Y. Hirose, T. Shimada, and T. Hasegawa, J. Appl. Phys. **105**, 123702 (2009).
[56] H. Kamisaka, T. Hitosugi, T. Hasegawa, T. Suenaga, and K. Yamashita, J. Chem. Phys. **131**, 034702 (2009).
[57] T. Hitosugi, H. Kamisaka, K. Yamashita, H. Nogawa, Y. Furubayashi, S. Nakao, N. Yamada, N. Chikamatsu, H. Kumigashira, M. Oshima, Y. Hirose, T. Shimada, and T. Hasegawa, Appl. Phys. Express **1**, 111203 (2008).
[58] D. Morris, Y. Dou, J. Rebane, C. E. J. Mitchell, R. G. Egdell, D. S. L. Law, A. Vittadini, and M. Casarin, Phys. Rev. B **61**, 13445 (2000).
[59] P. P. Edwards, A. Porch, M. O. Jones, D. V. Morgan, and R. M. Perks, Dalton Trans. 2995 (2004).
[60] T. J. Coutts, D. L. Young, and X. Li, MRS Bull. **25**, 58 (2000).
[61] R. J. Gonzalez, R. Zallen, and H. Berger, Phys. Rev. B **55**, 7014 (1997).
[62] I. Hamberg and C. G. Granqvist, J. Appl. Phys. **60**, R123 (1986).
[63] T. Gerfin and M. Grätzel, J. Appl. Phys. **79**, 1722 (1996).
[64] Y. Hirose, N. Yamada, S. Nakao, T. Hitosugi, T. Shimada, and T. Hasegawa, Phys. Rev. B **79**, 165108 (2009).
[65] Z. M. Jarzebski, Phys. Status Solidi A **71**, 13 (1982).
[66] T. Koida and M. Kondo, Appl. Phys. Lett. **89**, 082104 (2006).
[67] L. Raniero, I. Ferreira, A. Pimentel, A. Gonçalves, P. Canhola, E. Fortunato, and R. Martins, Thin Solid Films **511**, 295 (2006).
[68] H. Natsuhara, T. Ohashi, S. Ogawa, N. Yoshida, T. Itoh, S. Nonomura, M. Fukawa, and K. Sato, Thin Solid Films **430**, 253 (2003).
[69] M. Kambe, K. Sato, D. Kobayashi, Y. Kurokawa, Sh. Miyajima. M. Fukawa, N. Taneda, A. Yamada, and M. Konagai, Jpn. J. Appl. Phys. **45**, L291 (2006).